Second-order multiple-scattering theory associated with backscattering enhancement for a millimeter wavelength weather radar with a finite beam width

Satoru Kobayashi, Simone Tanelli, and Eastwood Im

Jet Propulsion Laboratory, California Institute of Technology, Pasadena, California, USA

Received 22 November 2004; revised 12 September 2005; accepted 28 September 2005; published 22 December 2005.

[1] Effects of multiple scattering on reflectivity are studied for millimeter wavelength weather radars. A time-independent vector theory, including up to second-order scattering, is derived for a single layer of hydrometeors of a uniform density and a uniform diameter. In this theory, spherical waves with a Gaussian antenna pattern are used to calculate ladder and cross terms in the analytical scattering theory. The former terms represent the conventional multiple scattering, while the latter terms cause backscattering enhancement in both the copolarized and cross-polarized components. As the optical thickness of the hydrometeor layer increases, the differences from the conventional plane wave theory become more significant, and essentially, the reflectivity of multiple scattering depends on the ratio of mean free path to radar footprint radius. These results must be taken into account when analyzing radar reflectivity for use in remote sensing.

Citation: Kobayashi, S., S. Tanelli, and E. Im (2005), Second-order multiple-scattering theory associated with backscattering enhancement for a millimeter wavelength weather radar with a finite beam width, *Radio Sci.*, *40*, RS6015, doi:10.1029/2004RS003219.

1. Introduction

[2] Millimeter wavelength weather radars have been extensively used to increase accuracy of measuring hydrometeor characteristics (e.g., raindrops, liquid cloud particles). In this frequency regime, multiple-scattering effects become important so as to be taken into account when using radar reflective intensity in retrieval algorithms of hydrometeor density. The occurrence of multiple scatterings was confirmed in 35 GHz radar measurements by the presence of depolarized signals reflected from spherical raindrops [*Ito et al.*, 1995; *Iguchi et al.*, 1992]. *Ito et al.* [1995] proposed an approximate analytical formula to calculate copolarized and depolarized intensities caused by second-order scattering in a single layer of hydrometeors for plane wave incidence. Since this formula is derived from the expansion of generalized spherical harmonics based on the time-dependent radiative transfer theory [*Oguchi*, 1980], it is particularly useful to the analysis with a short pulsed weather radar in remote sensing.

[3] From the early 1970s to the early 1990s, multiple scattering in randomly distributed particles was intensively studied through the analytical method of electromagnetic wave [*de Wolf*, 1971; *Golubentsev*, 1984; *Tsang and Ishimaru*, 1985; *Kravtsov and Saichev*, 1982]. In the course of study, two main contributions of multiple scattering to reflective intensity were revealed; one is the conventional multiple scattering called ladder term, and the other called cross term, is the contribution from interference of two ray paths mutually satisfying the condition of time reversal paths, as will be addressed in this paper. The contribution of a cross term is negligible to that of the corresponding ladder term unless the transmitting and receiving directions satisfy the nearly backscattering condition. Once this condition is satisfied, as is always the case of ground- based monostatic radars, the cross term becomes comparable to the ladder term, resulting in backscattering enhancement. However, for the case of spaceborne radars, we must not always expect the backscattering enhancement because the platform motion at a high speed introduces a significant displacement, breaking the right backscattering condition. If the scattering angle is far from backscattering, it is sufficient to consider only the ladder term. As *Barbanenkov et al.* [1991] and *Ishimaru* [1991] reviewed, the backscattering enhancement is a universal wave phenomenon observed whenever the multiple scattering is substantial. Therefore it is not appropriate to use the second-order scattering formula of *Ito et al.* [1995]

0048-6604/05/2004RS003219$11.00

for monostatic radars without evaluating the effect of backscattering enhancement.

[4] An application of backscattering enhancement to weather radars was studied for turbulent media by *Lure et al.* [1989]. However, for millimeter wavelength radars, *de Wolf et al.* [2000] and *Kobayashi* [2002] showed that the incoherent scattering from cloud particles carried by the turbulent air cannot be observed except for extreme case. Hence in this paper, only the scattering from each particle, namely delta function–like singular incoherent component will be considered. For this scattering component, backscattering enhancement was studied as a scalar theory [*Ishimaru and Tsang*, 1988; *Akkermans et al.*, 1986; *Barbanenkov and Ozrin*, 1988; *Golubentsev*, 1984; *Tsang and Ishimaru*, 1984, 1985] and as a vector theory [*Mandt et al.*, 1990; *Mandt and Tsang*, 1992; *Akkermans et al.*, 1988; *Stephen and Cwilich*, 1986; *Kuzmin et al.*, 1992; *Mishchenko*, 1991, 1992]. Numerical simulations for the vector theory were found in references [*Oguchi and Ihara*, 2005; *van Albada and Lagendijk*, 1987]. Among these vector theories, the perturbation theories [*Mandt et al.*, 1990; *Mandt and Tsang*, 1992; *Kuzmin et al.*, 1992; *Mishchenko*, 1991, 1992] can be considered more appropriate for hydrometeors because of its small volume fraction of scatterers of order of 10^{-5}, comparing with the diffusion theories [*Akkermans et al.*, 1988; *Stephen and Cwilich*, 1986]. Especially, two formalisms of *Mishchenko* [1991, 1992] and *Mandt et al.* [1990] are advantageous so as to have the explicit forms of scattering amplitude matrix in position space representation. The former formalism includes the contributions of ladder and cross terms of all orders, and seems to suit for numerical simulation, but not for analytical expression. The latter, on the other hand, includes at most the second-order terms, but it can give an analytically simple form for a system of a finite layer thickness. Furthermore the second-order theory can be considered to be sufficient for a dilute system such as hydrometeors as mentioned in references [*Ito et al.*, 1995; *Iguchi et al.*, 1992].

[5] In all the previous theoretical works, a plane wave is incident to a layer of randomly distributed particles, and the reflected wave is collected by a receiver at infinite range. On the other hand, in remote sensing, a spherical wave with a finite beam width, usually approximated as a Gaussian antenna pattern within the antenna mainlobe, is incident, and the reflected wave is received by an antenna at a finite range. For the single scattering, the plane wave theory can be applied to the spherical wave of a finite beam width with a slight correction on range and gain, as will be also shown in this paper. On the other hand, for multiple scattering, it is not appropriate to adopt the plane wave theory as it is, because a finite footprint radius can be considered to give a smaller reflectivity than the plane wave theory predicts, especially when the footprint radius is smaller than the mean free path of an illuminated body. The mean free path in a layer of hydrometeors can reach 1000–2000 m for millimeter wavelength wave, while a typical footprint radius is on order of hundreds meters for airborne applications, and a few kilometers for spaceborne cases. In this study, a time-independent multiple-scattering theory is formulated for a spherical wave along with a Gaussian antenna pattern, based on the plane wave theory of *Mandt et al.* [1990]. It means that the formalism of this paper can be applied to the stationary process such as CW radars (not FM-CW radars), but not to pulsed radars except for the special case described in section A3. To estimate amounts of the multiple scattering for pulsed radars in the general case, it is necessary to develop time-dependent algorithms as a future work, which are briefly discussed in section 4. Our analysis considers only a single layer of spherical water particles of uniform diameter and uniform number density. For simplicity of theoretical derivation, particles are assumed to be stationary in air throughout this paper. The limit of this last assumption will be discussed in section 3.

[6] The main purpose of this paper is to illustrate that reflectivity in multiple scattering for a finite beam width is smaller than the value predicted by the plane wave theory. The result will form the basis of a future retrieval algorithm of hydrometeors that takes a drop size distribution into consideration.

2. Formalism

[7] *Ishimaru and Tsang* [1988] derived a second-order multiple-scattering theory for anisotropic scatterers through the analytic method of electromagnetic wave approximated in scalar. A plane wave with infinite duration was used to lead a time-independent theory in which the thickness "d" of a layer is an adjustable parameter. *Mandt et al.* [1990] later expanded this scalar theory to a vector counterpart by introducing the three-dimensional characteristics of electromagnetic waves. In this section, the formalism of Ishimaru-Tsang and Mandt et al. is expanded to a spherical wave with a finite beam width represented by a Gaussian function. To deal with complication introduced by the finite beam width, further simplifications of integrals will be performed for the second-order ladder and cross terms as will be shown in this section and section A1.

2.1. First-Order Ladder Term

[8] As briefly mentioned in section 1, all the ladder terms are incorporated into radiative transfer theory. The first-order ladder term, corresponding to the conventional single scattering intensity, is depicted schematically in Figures 1a and 1b for a radar with finite beam width. To

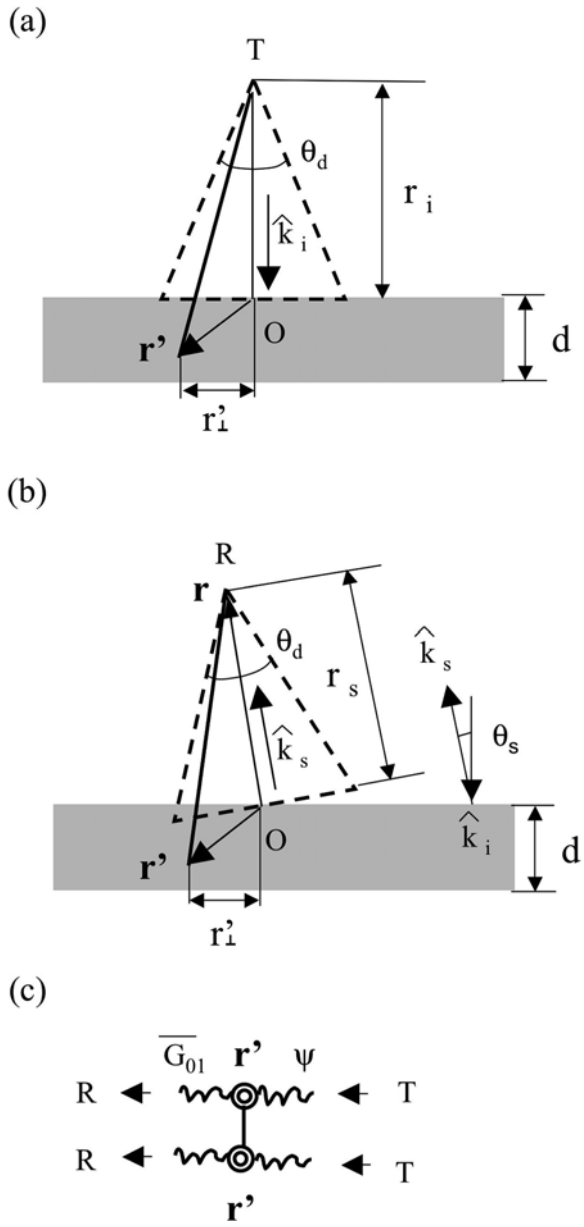

Figure 1. First-order ladder term. (a) Incident spherical wave emitting from a transmitting antenna T of 3 dB aperture angle θ_d. The wave scatters at $\mathbf{r}'$ in a layer of random medium of thickness d; $\hat{k}_i$ denotes a radar incident wave number. (b) Wave scattered at $\mathbf{r}'$ reaching a receiving antenna R of 3 dB aperture angle θ_d; $\hat{k}_s$ denotes a radar scattering wave number. (c) Diagram in which ψ denotes the incident spherical wave and $\overline{G}_{01}$ denotes a scattering Green function from $\mathbf{r}'$ to antenna R.

illustrate the backscattering enhancement, at first a bistatic radar is considered by assuming a small value of scattering angle $\theta_s \ll 1^\circ$ as shown in Figures 1a and b, and then the formula for monostatic radar is derived by taking the limit of $\theta_s \to 0$. In Figure 1a, the point O is the center of the footprint at the top boundary of the random medium layer. The unit vector $\hat{k}_i$ denotes the direction of the incident wave along the transmitting antenna axis TO, and the transmitting range r_i is the length of TO. When the incident spherical wave is scattered by a point scatterer at point $\mathbf{r}'$ in the medium, the field at point $\mathbf{r}'$ can be represented for a large range $r_i \gg |\mathbf{r}'|$ and a small 3 dB aperture angle $\theta_d \ll 1^\circ$ in the form of

$$\psi(\mathbf{r}') \approx \sqrt{P_t G_0 / 4\pi}\, r_i^{-1} \exp[ikr_i] \cdot \exp[i\boldsymbol{\kappa}_i \mathbf{r}'] \exp\left[-r_\perp'^2/4\sigma_r^2\right] \psi_0 \quad (1)$$

In equation (1), P_t, G_0 and k denote the total transmitting power, the center gain of the antenna, and the wave number in air, respectively. $r'_\perp$ denotes the transverse length of the point $\mathbf{r}'$ as shown in Figure 1. The 3 dB footprint radius σ_r can be defined as

$$\sigma_r^2 = r_i^2 \theta_d^2 / 2^3 \ln 2 \quad (2)$$

The vector $\boldsymbol{\psi_0}$ in equation (1) represents an initial polarization state. The effective incident wave number $\boldsymbol{\kappa_i}$ in the medium can be represented, based on work by *Ishimaru and Tsang* [1988]:

$$\boldsymbol{\kappa}_i \approx k\,\hat{k}_i - i\kappa_{iz}''\hat{z} \quad (3)$$

The incident direction $\hat{k}_i$ can be defined with polar coordinates as

$$\hat{k}_i = \sin\theta_i \cos\varphi_i \hat{x} + \sin\theta_i \sin\varphi_i \hat{y} + \cos\theta_i \hat{z} \quad (4)$$

in which the base vector $\hat{z}$ in the Cartesian system is taken in the zenith. The directions of $\hat{x}$ and $\hat{y}$ are arbitrary in the orthogonal plane to $\hat{z}$. In equation (3), the imaginary part κ_{iz}'' is represented in the form of

$$\kappa_{iz}'' = -\kappa_e/2 \cos\theta_i \quad (5)$$

Note that the negative signs in equations (3) and (5) have been chosen because of $\theta_i \approx \pi$. The extinction rate κ_e in equation (5) is defined by the Foldy-Twersky-Oguchi formula [*Oguchi*, 1973; *Tsang and Kong*, 2001]:

$$\kappa_e = Im\left[4\pi N_0 k^{-1} F\left(\hat{k}_i, \hat{k}_i\right)\right] \quad (6)$$

in which N_0 is the number density of hydrometeors. Since $F(\hat{k}_s, \hat{k}_i)$ denotes the scattering amplitude matrix scattered from the directions $\hat{k}_i$ to $\hat{k}_s$, $F(\hat{k}_i, \hat{k}_i)$ in equation (6) means the forward scattering amplitude matrix.

[9] The reflected wave from the point $\mathbf{r}'$ to the receiving antenna R of a bistatic radar system is depicted in Figure 1b. For simplicity, it is assumed that the receiving antenna R shares its footprint center O with the transmitting antenna T. The geometrical configuration of a spaceborne monostatic weather radar orbiting at an altitude of 350–400 km over the Earth surface with a speed of 7–8 km/sec can be approximated by the bistatic radar configuration depicted in Figure 1b, because the antenna moves by a large amount during the round trip time of pulse. The corresponding angle shift θ_s is approximately equal to 0.0025°. In rigor, we have to note that, for the spaceborne radar, the antenna gain at the receiving position changes from that at the transmitting position. However the difference in gain is generally negligible so that the above approximation is satisfied. For a small scattering angle $\theta_s \ll 1°$ along with the condition for the receiving range $r_s(\gg |\mathbf{r}'|)$, the Green function of the signal received by the antenna R, located at point $\mathbf{r}$, can be approximated in the form of

$$\bar{G}_{01}(\mathbf{r}, \mathbf{r}') \approx \sqrt{\pi G_0 / k^2}\, r_s^{-1} \exp[ikr_s] \cdot \exp[-i\boldsymbol{\kappa}_s \mathbf{r}'] \exp\left[-r_\perp'^2/4\sigma_r^2\right] \bar{I}_2 \tag{7}$$

in which the two dimensional identical operator/dyad is defined with bra-ket notations in quantum mechanics as

$$\bar{I}_2 = \left|\hat{\theta}\right\rangle\left\langle\hat{\theta}\right| + \left|\hat{\varphi}\right\rangle\left\langle\hat{\varphi}\right| \tag{8}$$

In equation (8), the unit vectors in the polar and azimuth directions are represented by $\hat{\theta}$ and $\hat{\varphi}$ respectively. The effective scattered wave number $\boldsymbol{\kappa}_s$ in the medium can be defined in a similar manner to equations (3) and (5):

$$\boldsymbol{\kappa}_s \approx k\,\hat{k}_s + i\kappa_{sz}''\hat{z} \tag{9}$$

with

$$\hat{k}_s = \sin\theta_s \cos\varphi_s \hat{x} + \sin\theta_s \sin\varphi_s \hat{y} + \cos\theta_s \hat{z} \tag{10}$$

$$\kappa_{sz}'' = \kappa_e/2 \cos\theta_s \tag{11}$$

The scattering process in Figures 1a and 1b is represented by the Dyson's diagram in Figure 1c. For completely random distributions of a uniform density N_0 (i.e., no particle-particle correlation), the first-order ladder term intensity can be represented via the diagram of Figure 1c in the integral form:

$$I_L^{(1)} = (4\pi)^2 N_0 \int_{-d}^{0} dz \int d\mathbf{r}'_\perp\, \psi^\dagger(\mathbf{r}')\, F^\dagger\left(\hat{k}_s, \hat{k}_i\right) \cdot \bar{G}_{01}^\dagger(\mathbf{r}, \mathbf{r}')\, \bar{G}_{01}(\mathbf{r}, \mathbf{r}')\, F\left(\hat{k}_s, \hat{k}_i\right) \psi(\mathbf{r}') \tag{12}$$

in which the superscript † indicates the complex conjugate of a dyad or a vector.

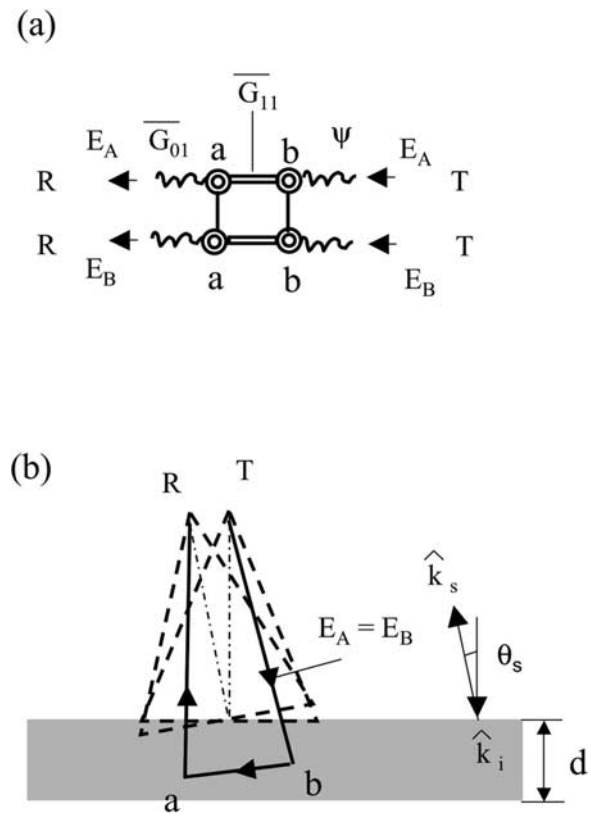

Figure 2. Second-order ladder term. An incident field E_A and its identical conjugate field E_B emit from antenna T and scatter at points b and a successively in the random medium, being received by antenna R. (a) Diagram in which $\overline{G}_{11}$ is a Green function in the medium. (b) Geometrical configuration.

[10] Substitutions of equations (1) and (7) into equation (12) yield for nearly backscattering condition,

$$I_L^{(1)} \approx P_t G_0^2 \lambda^2 \theta_d^2 \left(2^7 \pi \ln 2\, r_s^2\right)^{-1} N_0 \left\{2\left(\kappa_{iz}'' + \kappa_{sz}''\right)\right\}^{-1} \cdot \sum_{\hat{\alpha}} \left|\left\langle\hat{\alpha}\middle|F\left(-\hat{k}_i, \hat{k}_i\right)\middle|\psi_0\right\rangle\right|^2 \cdot \left\{1 - \exp\left[-2\left(\kappa_{iz}'' + \kappa_{sz}''\right) d\right]\right\} \tag{13}$$

where the approximation of $r_s \approx r_i$ and $\hat{k}_s \approx -\hat{k}_i$ have been used. In equation (13), the summation over unit vector $\hat{\alpha}$ is taken over a complete set of polarizations such as the $\hat{h}$ and $\hat{v}$ directions. When the initial polarization is in the $\hat{v}$ direction and the absorption is negligible, equation (13) projected onto the $\hat{v}$-polarized component can be written in the form of

$$I_L^{(1)} = P_t G_0^2 \lambda^2 \theta_d^2 \left(2^9 \pi^2 \ln 2\, r_s^2\right)^{-1} \xi_{bak}\, d \tag{14}$$

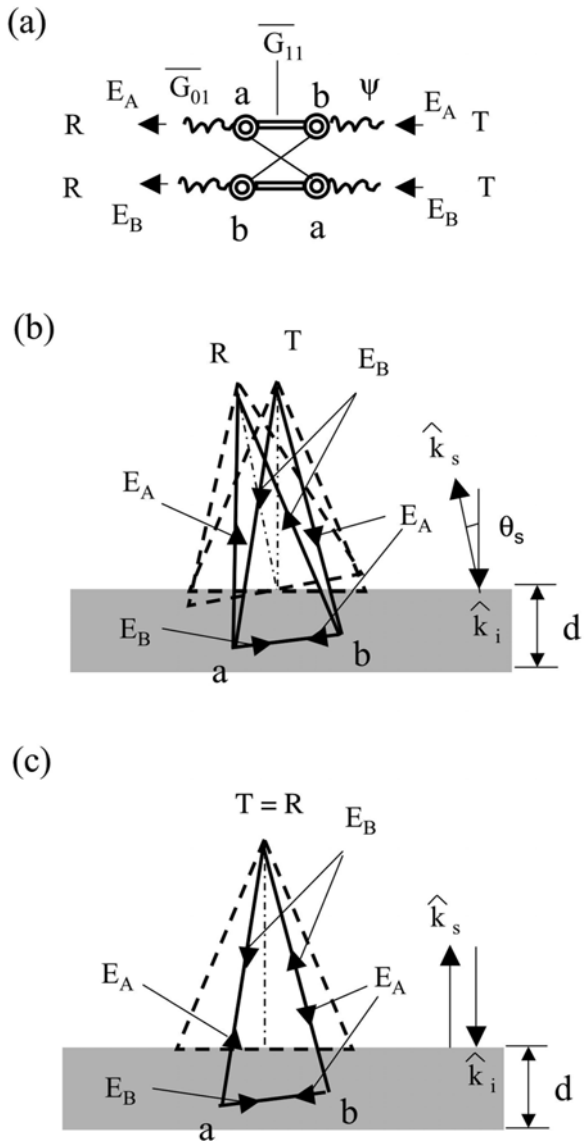

Figure 3. Second-order cross term. An incident field E_A takes the same path as in Figure 2b, while the conjugate field E_B emits from antenna T and scatters at points a and b successively, being received by antenna R. (a) Diagram. (b) General scattering $\theta_s \neq 0$. (c) Backscattering $\theta_s = 0$, where E_B takes the time reversal path of E_A.

where the volumetric backscattering reflectivity $\xi_{bak} = 4\pi\ N_0|F_{\hat{v}\hat{v}}(-\hat{k}_i,\ \hat{k}_i)|^2$ has been introduced. If the layer thickness d is replaced with the longitudinal resolution length $c\tau/2$, we can retrieve the radar equation for volume scattering with a pulse duration of τ. Hence the first-order ladder term for a small scattering angle $\theta_s \ll 1°$ has been proven to be equivalent to the radar equation as expected.

2.2. Second-Order Ladder Term

[11] The second-order ladder term for bistatic radars can be represented by the diagram in Figure 2a, and the corresponding geometry is represented by Figure 2b. The field E_A and its identical conjugate field E_B are transmitted from the antenna T. These fields first scatter at point b and, then at point a, eventually returning to the receiving antenna R. Under the condition that the mean free path of the medium is much larger than the wavelength, which is almost always satisfied for hydrometeors, a Green function in the medium can be approximated from a complete form of *van Bladel* [1961]

$$\bar{G}_{11}(\mathbf{r},\ \mathbf{r}') \approx (4\pi)^{-1}|\mathbf{r}-\mathbf{r}'|^{-1}\exp[ik|\mathbf{r}-\mathbf{r}'|]\,\bar{I}_2 \quad (15)$$

Substituting equations (1), (7), and (15) into the integral form corresponding to the diagram in Figure 2a, the second-order ladder term for the finite beam width can be derived as shown in Appendix A1:

$$\begin{aligned} I_L^{(2)} = {} & P_t G_0^2 \lambda^2 \theta_d^2 \left(2^7 \pi\ \ln 2\, r_s^2\right)^{-1} N_0^2 \left\{2\left(\kappa_{iz}'' + \kappa_{sz}''\right)\right\}^{-1} \\ & \cdot \int_0^\infty d\eta \int_0^{2\pi} d\varphi \int_0^d d\zeta \frac{\eta}{1+\eta^2} \\ & \cdot \exp\left[-\kappa_e\sqrt{1+\eta^2}\,\zeta\right]\ \exp\left[-\zeta^2\eta^2/4\sigma_r^2\right] \\ & \cdot \sum_{\hat{\alpha}} \left\{ \left| \left\langle \hat{\alpha} \middle| F\left(\hat{k}_s,\ \hat{r}\right) F\left(\hat{r},\ \hat{k}_i\right) \middle| \psi_0 \right\rangle \right|^2 \right. \\ & \cdot \left[\exp\left\{-2\kappa_{iz}''\zeta\right\} - \exp\left\{2\kappa_{sz}''\zeta - 2\left(\kappa_{iz}'' + \kappa_{sz}''\right)d\right\}\right] \\ & + \left| \left\langle \hat{\alpha} \middle| F\left(\hat{k}_s,\ -\hat{r}\right) F\left(-\hat{r},\ \hat{k}_i\right) \middle| \psi_0 \right\rangle \right|^2 \\ & \left. \cdot \left[\exp\left\{-2\kappa_{sz}''\zeta\right\} - \exp\left\{2\kappa_{iz}''\zeta - 2\left(\kappa_{iz}'' + \kappa_{sz}''\right)d\right\}\right] \right\} \end{aligned} \quad (16)$$

where $\eta \equiv \tan\theta$ has been defined. The variables θ and φ are polar coordinates for the directional variable $\hat{r}$ that is defined inside the argument of the scattering amplitude matrix F. The other integral variable $\zeta \equiv z_a - z_b$ is the relative coordinate in the direction of layer thickness (See the details in Appendix A1). The second-order ladder term corresponds to the conventional second-order scattering derived by the radiative transfer theory.

2.3. Second-Order Cross Term

[12] The diagram of the second-order cross term is depicted in Figure 3a. The direction of the conjugate field is arbitrary. In this paper, the notation of the direction of the fields will follow that of *Kravtsov and Saichev* [1982]. In the geometry of Figure 3b, the field

E_A travels in the same path as that in Figure 2b, while the conjugate field E_B, starting from the transmitting antenna T, scatters first at point a and, then at point b, eventually returning to the receiving antenna R. Since the fields E_A and E_B have different path lengths, random distributions of points a and b will cause strong decorrelation, generally giving negligible contribution to the measured intensity. However for the backscattering measurement ($\theta_s = 0$) depicted in Figure 3c, the fields E_A and E_B have the same path lengths, giving finite correlation that leads to backscattering enhancement. The ray path of E_B in Figure 3c is referred to as the time reversal path of E_A. As the transmitting and receiving gains are assumed to be symmetric in this study, the received fields E_A and E_B have also the same magnitudes. Although this assumption is not indispensable to obtain the backscattering enhancement, it is assumed for the sake of simplicity in calculation.

[13] The second-order cross term for the finite beam width can be derived in a similar manner to the second-order ladder term. The result is

$$
\begin{aligned}
I_C^{(2)} = {} & P_t G_0^2 \lambda^2 \theta_d^2 \left(2^7 \pi \ln 2\, r_s^2\right)^{-1} N_0^2 \left(\kappa_{iz}'' + \kappa_{sz}''\right)^{-1} \\
& \cdot \int_0^\infty d\eta \int_0^{2\pi} d\varphi \int_0^d d\zeta \frac{\eta}{1+\eta^2} \\
& \cdot \exp\left[-\left\{\kappa_e \sqrt{1+\eta^2} + \kappa_{iz}'' + \kappa_{sz}''\right\}\zeta\right] \\
& \cdot \exp\left[-\zeta^2\eta^2/4\sigma_r^2\right] \left\{1 - \exp\left[-2\left(\kappa_{iz}'' + \kappa_{sz}''\right)\right.\right. \\
& \left.\left. \cdot (d-\zeta)\right]\right\} Re\left[\left\{\sum_{\hat{\alpha}} \left\langle \hat{\alpha} \middle| F\left(\hat{k}_s, \hat{r}\right) F\left(\hat{r}, \hat{k}_i\right) \middle| \psi_0 \right\rangle^* \right.\right. \\
& \left.\left. \cdot \left\langle \hat{\alpha} \middle| F\left(\hat{k}_s, -\hat{r}\right) F\left(-\hat{r}, \hat{k}_i\right) \middle| \psi_0 \right\rangle \right\} \exp[i(k_{dz} + t)\zeta]\right]
\end{aligned}
\tag{17}
$$

in which the deviation vector $\mathbf{k_d}$ from the backscattering direction and the new variable t have been introduced on the basis of work by *Ishimaru and Tsang* [1988]:

$$
\mathbf{k_d} = k\left(\hat{k}_s + \hat{k}_i\right) \equiv k_{dx}\hat{x} + k_{dy}\hat{y} + k_{dz}\hat{z} \tag{18}
$$

$$
t \equiv k_{dx}\eta\cos\varphi + k_{dy}\eta\sin\varphi \tag{19}
$$

Note that the second-order ladder term (equation (16)) and cross term (equation (17)) can be reduced to the forms of *Mandt et al.* [1990] in the limit of $\sigma_r \to \infty$. However an advantage of the form of equation (17) is that the decorrelation caused by increase in the value of $\mathbf{k_d}$ is explicitly represented through the term $\exp[i(k_{dz} + t)\zeta]$. Another advantage is that equation (17) is represented in real valued form.

[14] Since *Mandt et al.* [1990] did not elaborate on the relation between the ladder and cross terms in the second order for the case of backscattering $\theta_s = 0$, we shall derive it. For the backscattering, the following conditions are satisfied for equations (16) and (17):

$$
\hat{k}_s = -\hat{k}_i \tag{20}
$$

$$
\kappa_{iz}'' = \kappa_{sz}'' \tag{21}
$$

$$
t = k_{dz} = 0 \tag{22}
$$

In general, a scattering amplitude matrix F satisfies the Saxon's reciprocal relation [*Mishchenko*, 1991; *Saxon*, 1955]:

$$
F(-\hat{n}, -\hat{n}') = QF^t(\hat{n}', \hat{n})Q \tag{23}
$$

where the superscript t denotes matrix transpose, and the matrix Q is defined as

$$
Q = \begin{bmatrix} 1 & 0 \\ 0 & -1 \end{bmatrix} \tag{24}
$$

Without losing generality, we can assume the initial polarization:

$$
\psi_0 \equiv \hat{v} = \begin{bmatrix} 1 \\ 0 \end{bmatrix} \tag{25}
$$

Using equations (20) and (23) and the fact of $\langle \mathbf{a}|A|\mathbf{b}\rangle = \langle \mathbf{b}|A^\dagger|\mathbf{a}\rangle^*$, we can show

$$
\left\langle \hat{v} \middle| F\left(\hat{k}_s, -\hat{r}\right) F\left(-\hat{r}, \hat{k}_i\right) \middle| \hat{v} \right\rangle = \left\langle \hat{v} \middle| F\left(\hat{k}_s, \hat{r}\right) F\left(\hat{r}, \hat{k}_i\right) \middle| \hat{v} \right\rangle \tag{26}
$$

Inserting equations (21), (22), and (26) into equations (16) and (17), we see for the copolarized component that the cross term is equal to the ladder term:

$$
I_c^{(2)}(CO) = I_L^{(2)}(CO) \tag{27}
$$

where CO stands for the copolarized component. On the other hand, for the cross polarized component, it is impossible to deduce a simple relation from equations (16) and (17) unless additional symmetries exist in a system. These results are in agreement with general formulas of *Mishchenko* [1991, 1992].

[15] For the Mie scattering of spherical particles, the matrix $F(\hat{k}_s, \hat{r})\ F(\hat{r}, \hat{k}_i)$ can be shown to have an

antisymmetric form for the backscattering condition ($\hat{k}_i = -\hat{k}_s$) [*Tazaki et al.*, 2000]:

$$F\left(\hat{k}_s, \hat{r}\right) F\left(\hat{r}, \hat{k}_i\right) = \begin{bmatrix} a\cos 2\varphi + b & a\sin 2\varphi \\ -a\sin 2\varphi & a\cos 2\varphi - b \end{bmatrix} \tag{28}$$

in which

$$a \equiv [f_{11}(\theta - \theta_s) f_{11}(\theta_i - \theta) + f_{22}(\theta - \theta_s) f_{22}(\theta_i - \theta)]/2 \tag{29}$$

$$b \equiv [f_{11}(\theta - \theta_s) f_{11}(\theta_i - \theta) - f_{22}(\theta - \theta_s) f_{22}(\theta_i - \theta)]/2 \tag{30}$$

and $f_{11}(\theta)$ and $f_{22}(\theta)$ are the components of Mie scattering amplitude matrix. Alternatively, we can write equation (28) as

$$\left\langle \hat{h} \middle| F\left(\hat{k}_s, \hat{r}\right) F\left(\hat{r}, \hat{k}_i\right) \middle| \hat{v} \right\rangle = -\left\langle \hat{v} \middle| F\left(\hat{k}_s, \hat{r}\right) F\left(\hat{r}, \hat{k}_i\right) \middle| \hat{h} \right\rangle \tag{31}$$

Using equations (20), (23), and (31), we can show for the cross polarized component scattered from $\hat{v}$ to $\hat{h}$:

$$\left\langle \hat{h} \middle| F\left(\hat{k}_s, \hat{r}\right) F\left(\hat{r}, \hat{k}_i\right) \middle| \hat{v} \right\rangle = \left\langle \hat{h} \middle| F\left(\hat{k}_s, -\hat{r}\right) F\left(-\hat{r}, \hat{k}_i\right) \middle| \hat{v} \right\rangle \tag{32}$$

Inserting equations (21), (22), and (32) into equations (16) and (17), we can derive the equality between the ladder and cross terms in cross polarization for spherical particles:

$$I_c^{(2)}(CX) = I_L^{(2)}(CX) \tag{33}$$

where *CX* stands for the cross polarized component. A recent numerical simulation by *Oguchi and Ihara* [2005] further reported that for cross polarization, the equality $C^{cx} = L^{cx}$ is satisfied only to the second order.

3. Results and Discussion

[16] Multiple scatterings including backscattering enhancement can be considered to effectively increase radar reflectivity. When hydrometeors consist of spherical particles, the first-order ladder term $I_L^{(1)}$ has only the copolarized component, that is, $I_L^{(1)} = I_L^{(1)}(CO)$. Furthermore $I_L^{(1)}$ is almost constant in the vicinity of $\theta_s = 0$ ($\theta_s < 0.3°$), within which the backscattering enhancement occurs. For this reason, the intensity of a multiple-scattering term will be normalized by $I_L^{(1)}$ to be converted to an effective reflectivity in the rest of this paper. For instance, the second-order ladder reflectivity in copolarized component L_2^{co} will mean $I_L^{(2)}(CO)/I_L^{(1)}$.

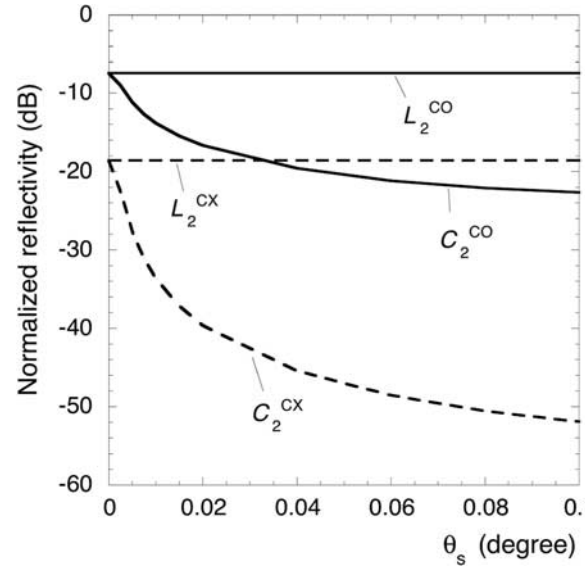

Figure 4. Reflectivities normalized by the single-scattering intensity versus the scattering angle θ_s taken in the plane parallel to the initial polarization. The reflectivities of the ladder term L_2^{co} and the cross term C_2^{co} in copolarization are represented by solid lines, and those of the ladder term L_2^{cx} and the cross term $C_2{}^{cx}$ in cross polarization are represented by dashed lines. Spherical water particles of diameter D = 1 mm, particle number density $N_0 = 5 \times 10^3$ m^{-3}, and layer thickness d = 100 m are used, which give the mean free path l_0 = 77.2 m, the optical thickness τ_d = 1.30, and the normalized footprint radius σ_r/l_0 = 0.288.

[17] The reflectivities of the second-order terms for a finite beam width can be numerically calculated through equations (16) and (17). In Figure 4, the reflectivities of the ladder term L_2^{co} and the cross term C_2^{co} in copolarization (solid lines), and those of the ladder term L_2^{cx} and the cross term C_2^{cx} in cross polarization (dashed lines) are plotted as a function of the bistatic scattering angle θ_s. Here θ_s is taken in the plane parallel to the initial polarization. The results are presented for the 3 dB aperture angle $\theta_d = 0.3°$, and the range r_s = 10 km, corresponding to the footprint radius σ_r = 22.2 m. Radiation frequency is set at 95 GHz. The random medium is a single layer with thickness d = 100 m, constituted of spherical water drops with particle number density $N_0 = 5 \times 10^3$ m^{-3} and uniform diameter D = 1 mm. These parameters result in the single-particle albedo of 0.53 (i.e., the total scattering cross section divided by the total extinction cross section), the mean free path $l_0 \equiv$

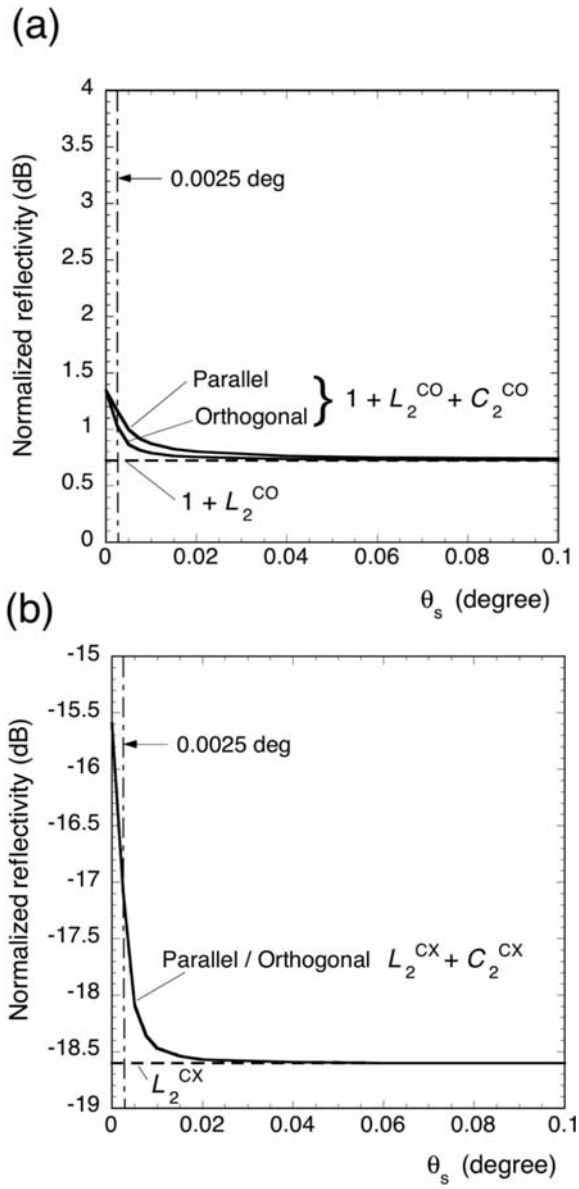

Figure 5. Normalized reflectivities summed from the first- to second-order terms as functions of the scattering angle θ_s. Here θ_s is taken in one of two planes that are parallel and orthogonal to the initial polarization, referred to as parallel and orthogonal angular displacements, respectively. The same parameters as in Figure 4 are used. A typical displacement angle $\theta_s = 0.0025°$ for spaceborne radars is marked by the vertical dash-dotted lines. (a) Copolarization. The parallel and orthogonal angular displacements show spatial anisotropy for $1 + L_2^{co} + C_2^{co}$ (solid lines) but not for $1 + L_2^{co}$ (dash-dotted line). (b) Cross polarization. The parallel and orthogonal angular displacements show no spatial anisotropy for $L_2^{cx} + C_2^{cx}$.

$\kappa_e^{-1} = 77.2$ m, the optical thickness $\tau_d \equiv \kappa_e d = 1.30$, and the normalized footprint radius $\sigma_r/l_0 = 0.288$. On the basis of a scalar theory including all the ladder and cross terms [*Ishimaru and Tsang*, 1988; *Tsang and Kong*, 2001], truncation at the second order can be considered valid in this range of albedo and optical thickness. Unless specified otherwise, theses parameters will be used in the remainder of this section.

[18] Figure 4 shows that the ladder terms L_2^{co} (solid) and L_2^{cx} (dashed) are practically constant for $\theta_s < 0.1°$ for the above parameters. The cross terms C_2 are equal to the ladder terms L_2 at $\theta_s = 0$ in both polarizations. These results are theoretically expected from equations (27) and (33). As θ_s increases, the cross terms rapidly decreases because of the term $\exp[i(k_{dz} + t)\zeta]$ in equation (17), as described in section 2.3. This rapid reduction in reflectivity is more evident for the cross polarization than for the copolarization. It is noted that the constancy of L_2 and the decaying behavior of C_2 in both polarizations in Figure 4 will hold even when changing either the beam width θ_d or the range r_s, correspondingly changing the footprint radius σ_r. Behaviors of L_2 and C_2 as functions of σ_r, including the relation to the plane wave theory, will be studied for fixed values of θ_s in later figures.

[19] From an operational perspective, it is useful to compare the copolarized return intensity including the cross term, $1 + L_2^{co} + C_2^{co}$, to the conventional return intensity $1 + L_2^{co}$. These values were calculated in Figure 5 for two conditions referred to as parallel and orthogonal angular displacements respectively. Suppose that the scattering plane is parallel to the $\hat{v}$ direction. In the parallel angular displacement, the initial polarization ψ_0 is chosen in the $\hat{v}$ direction, while in the orthogonal one, ψ_0 is in the direction $\hat{h}$. In Figure 5a, the values of $1 + L_2^{co}$(dotted line) for these two conditions coincide, while the values of $1 + L_2^{co} + C_2^{co}$(solid lines) for the two conditions coincide only at $\theta_s = 0$. As θ_s increases, the values of the parallel angular displacement show slower decay than those of the orthogonal angular displacement, indicating that the C_2^{co} term is anisotropic in copolarization. Since there is no return of the first-order scattering in cross polarization, that is, $I_L^{(1)}(CX) = 0$, the total cross polarized return is represented by L_2^{cx} or $L_2^{cx} + C_2^{cx}$, which is equal to linear depolarization ratio (LDR). These values are plotted in Figure 5b, in which not only the term L_2^{cx} but also the term $L_2^{cx} + C_2^{cx}$ coincide to each other between the parallel and vertical angular displacements, providing no spatial anisotropy. The results of the spatial anisotropy near the backscattering direction, shown in Figures 5a and 5b, are in agreement with the works of *van Albada and Lagendijk* [1987] and *van Albada et al.* [1987], who first attributed the anisotropy to the vector property of electromagnetic wave through computer simulation without theoretical confirmation.

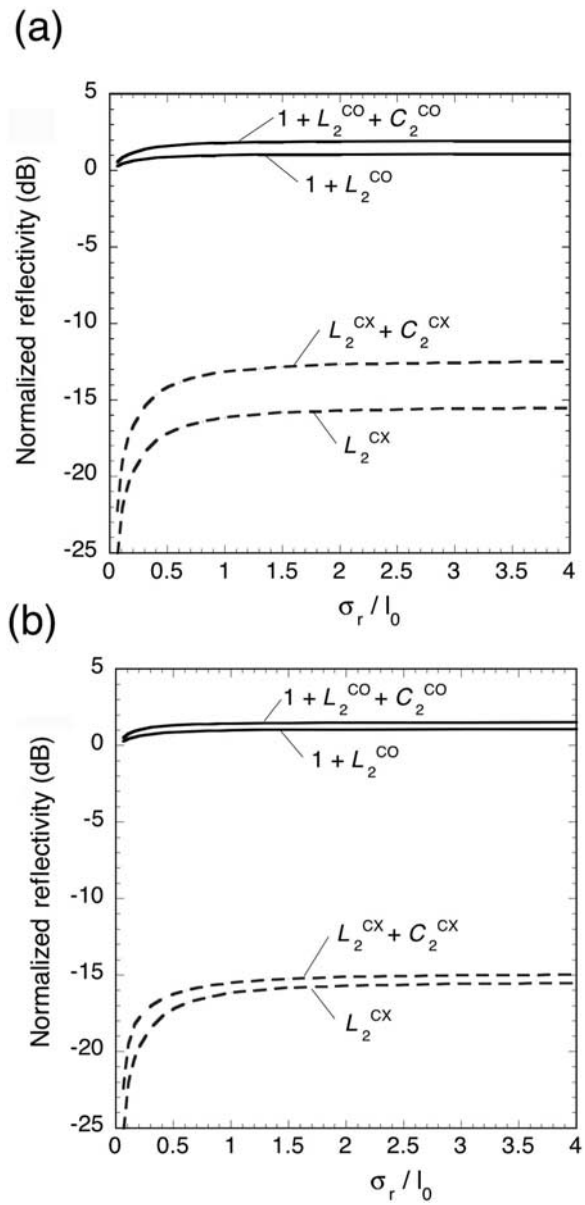

Figure 6. Normalized reflectivities as functions of the normalized footprint radius σ_r/l_0. Solid and dashed lines represent the reflectivities in copolarization and cross polarization, respectively. The same parameters as in Figure 4 are used. Note that $\sigma_r/l_0 \gg 1$ corresponds to the plane wave theory. (a) Backscattering $\theta_s = 0$. (b) Biscattering in a spaceborne radar with $\theta_s = 0.0025°$.

The features of this spatial anisotropy, including its origin, are derived in Appendix A2. Regardless of the angular displacements, the backscattering enhancements appear with angular widths of the order of $2\pi\kappa_e/k \approx 0.002°$, which is in agreement with the previous plane wave theories [*Barbanenkov et al.*, 1991; *de Wolf*, 1971; *Ishimaru*, 1991; *Kuzmin et al.*, 1992; *Tsang and Kong*, 2001; *van Albada and Lagendijk*, 1987] and plane wave experiments [*Akkermans et al.*, 1986; *Kuga and Ishimaru*, 1984; *van Albada et al.*, 1987; *Wolf and Maret*, 1985]. The spatial anisotropy of reflectivity in remote sensing can thus be summarized as follows. As long as spherical particles are observed with ground-based monostatic radars, the anisotropy of reflectivity in copolarization does not appear because of its scattering angle $\theta_s = 0$. For bistatic radars, including spaceborne monostatic radars with $\theta_s \approx 0.0025°$, we must consider this effect. For simplicity of discussion in the rest of paper, only the parallel angular displacement will be considered.

[20] The dependence of multiple-scattering reflectivities on footprint radius σ_r is illustrated in Figure 6. The terms $1 + L_2^{co} + C_2^{co}$, $1 + L_2^{co}$ in copolarization (solid lines), and the terms $L_2^{cx} + C_2^{cx}$ and L_2^{cx} in cross polarizations (dashed lines) are plotted as a function of σ_r/l_0 in Figure 6a for the backscattering angle, that is, $\theta_s = 0$, and in Figure 6b for $\theta_s = 0.0025°$. The value σ_r/l_0 means that the footprint radius σ_r is normalized by the mean free path $l_0 = 77.2$ m. Note that neither the 3 dB aperture angle θ_d nor the range r_s are defined explicitly, since they are interrelated to σ_r in equation (2). In Figure 6, calculation is terminated at $\sigma_r/l_0 = 0.064$, that is, $\sigma_r = 5$ m, because in such a small footprint radius, the numerical integral in equation (17) does not converge with good accuracy for $\theta_s = 0.0025°$. Above $\sigma_r/l_0 \approx 2.5$, all the reflectivities in Figures 6a and 6b can be regarded as nearly constant, asymptotically approaching to the values that the plane wave theory [*Mandt et al.*, 1990] predicts. The return intensity with only the ladder terms, $1 + L_2^{co}$ (bottom solid line) and L_2^{cx} (bottom dashed line) in Figure 6b, are identical to those in Figure 6a, while the return intensity including the cross terms, $1 + L_2^{co} + C_2^{co}$ (top solid line) and $L_2^{cx} + C_2^{cx}$ (top dashed line) in Figure 6b, come to lower values than those of Figure 6a because of reduction of backscattering enhancement. For instance, choosing the same value of $\sigma_r/l_0 = 0.288$ as taken for Figure 5, the readings of $1 + L_2^{co} + C_2^{co}$ and $L_2^{cx} + C_2^{cx}$ in Figure 6a are 1.34 and -15.6 dB, corresponding to the values at $\theta_s = 0°$ in Figures 5a and 5b, respectively. Those readings at $\sigma_r/l_0 = 0.288$ in Figure 6b reduce to 1.16 and -17.1 dB, corresponding the values at $\theta_s = 0.0025°$ in Figures 5a and 5b, respectively.

[21] Since the normalized reflectivity of the first-order term is ever defined as unity for any σ_r/l_0, working as a constant bias, it is reasonable to study the effect of only the second-order terms. Figure 7 show the calculated values of $L_2^{co} + C_2^{co}$ and $L_2^{cx} + C_2^{cx}$ with a solid and a dashed line respectively. The monostatic radar is our main concern so that only the backscattering $\theta_s = 0$ will

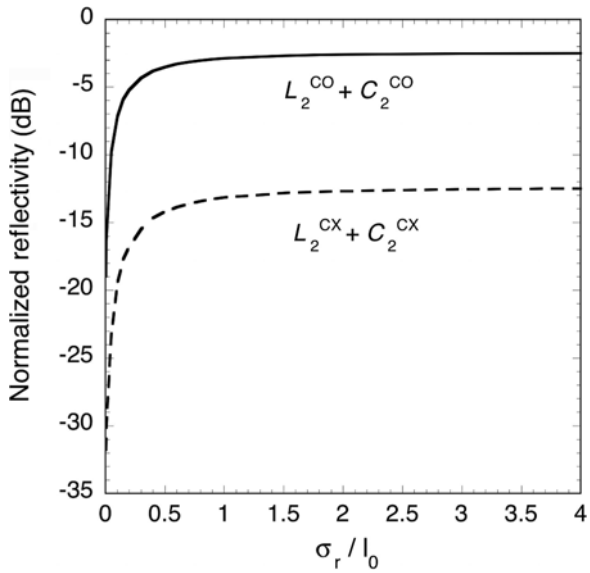

Figure 7. Reflectivity $L_2^{co} + C_2^{co}$ in copolarization (solid line) and the reflectivity $L_2^{cx} + C_2^{cx}$ in cross polarization (dashed line) as functions of the normalized footprint radius σ_r/l_0 for the backscattering $\theta_s = 0$. The same parameters as in Figure 4 are used. Note that only for $\theta_s = 0$, we can alternatively interpret the hydrometeor parameters as the two parameters defined by particle diameter $D = 1$ mm and the optical thickness $\tau_d = 1.30$ regardless of particle number density N_0 and layer thickness d. In $\sigma_r/l_0 < 1$, the reflectivities reduce to be far from the values predicted by the plane wave theory represented by $\sigma_r/l_0 \gg 1$.

be considered hereinafter. In Figure 7, both polarizations show rapid reductions in the region $\sigma_r/l_0 < 1$, while they asymptotically approach to the values of the plane wave theory as σ_r/l_0 increases, as already seen in Figure 6. It is noted that for $\theta_s = 0$, the values of equations (13), (16), and (17) can be shown to be independent of the particle number density N_0, when the layer thickness d and the footprint radius σ_r are normalized to the mean free path l_0. In this sense, we can alternatively interpret the hydrometeor parameters in Figure 7 as the two parameters defined by the particle diameter $D = 1$ mm and the optical thickness of layer $\tau_d = d/l_0 = 1.30$ regardless of the values of N_0 and d. For ease of readers' reference, the mean free path l_0 is plotted for $D = 1$ mm as a function of N_0 in Figure 8.

[22] In Figure 9, the terms $L_2^{co} + C_2^{co}$ (solid lines) and $L_2^{cx} + C_2^{cx}$ (dashed lines) are plotted as a function of optical thickness $\tau_d = d/l_0$ for several values of normalized footprint radius σ_r/l_0. Here only the frequency of 95 GHz and the particle diameter $D = 1$ mm are fixed. Since the mean free path l_0 is uniquely defined for a given particle density N_0, the value of τ_d should be considered to change by varying the physical layer thickness d. In both polarizations, the reflectivities become less sensitive to increments in τ_d, as the parameter σ_r/l_0 decreases. This is conspicuous for the cross polarization, in which the multiple-scattering amplitude factors such as $F(\hat{k}_s, \hat{r})\ F(\hat{r}, \hat{k}_i)$ with $\hat{r} = (\theta, \varphi)$ have high values around $\theta = 90°$ for nearly Rayleigh scattering regime. Hence the second-order scattering in the cross polarization is not so sensitive to increment in τ_d that is along the direction of $\theta = 0$ and 180°, but sensitive to increment in σ_r/l_0 that is along the direction of $\theta = 90°$. In fact, Figures 7 and 9 show that for a fixed τ_d, as σ_r/l_0 increases, the corresponding increment in the reflectivities of the cross polarization is larger than that of the copolarization.

[23] Using Figure 9, we can determine the reduction factor from the plane wave theory (i.e., $\sigma_r/l_0 = \infty$) for the particle diameter $D = 1$ mm, and given a footprint radius σ_r, a layer thickness d, and a particle number density N_o. Figure 9 also indicates that the plane wave theory can be applied to a smaller value of σ_r/l_0, as the optical thickness τ_d decreases. For example, at a large optical thickness $\tau_d = 4.0$, the values of $L_2^{co} + C_2^{co}$ (Solid lines) are -1.89 dB and -2.39 dB for $\sigma_r/l_0 = \infty$ and $\sigma_r/l_0 = 1$ respectively. These values reduce to -11.49 dB and -11.58 dB respectively at a small optical thickness $\tau_d = 0.05$. Hence the difference in $L_2^{co} + C_2^{co}$ between $\sigma_r/l_0 = \infty$ and $\sigma_r/l_0 = 1$ is 0.50 dB at $\tau_d = 4$, while it becomes only 0.09 dB at $\tau_d = 0.05$. It means that the plane wave theory can be approximately applied for the footprint radius $\sigma_r/l_0 = 1$ at the small optical thickness $\tau_d = 0.05$.

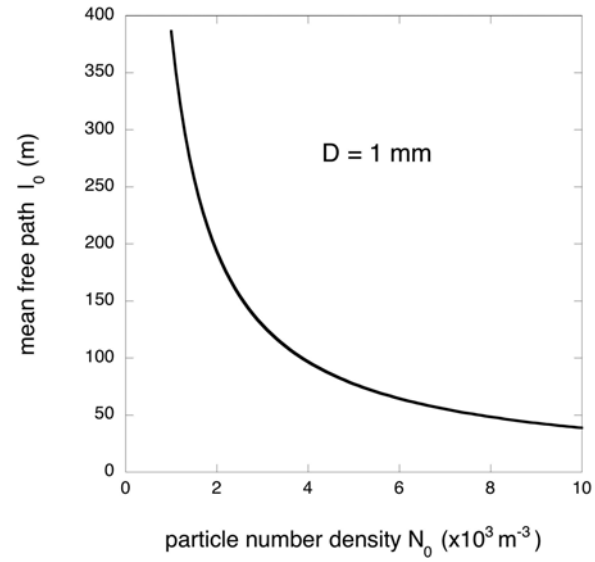

Figure 8. Mean free path l_0 versus particle number density N_0 for spherical water of diameter $D = 1$ mm.

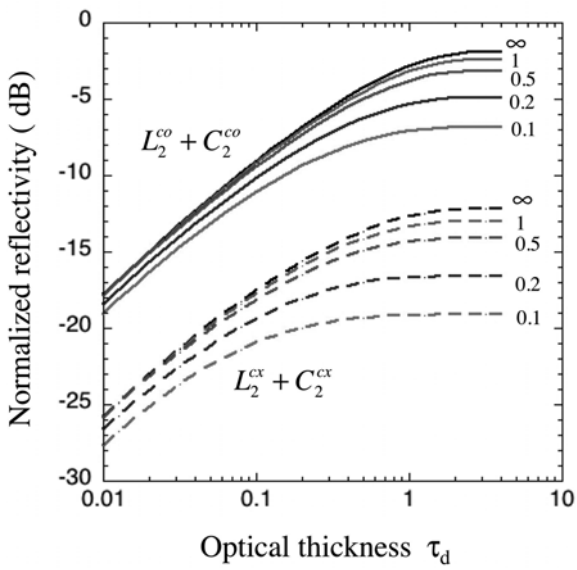

Figure 9. Reflectivity $L_2^{co} + C_2^{co}$ in copolarization (solid lines) and the reflectivity $L_2^{cx} + C_2^{cx}$ in cross polarization (dashed lines) as functions of the optical thickness τ_d for the backscattering $\theta_s = 0$. Hydrometeor diameter is set at $D = 1$ mm. Particle number density N_0 is set at an arbitrary value. The parameters of footprint radius σ_r/l_0 are set at (top to bottom) ∞, 1, 0.5, 0.2, and 0.1. The differences of finite footprint radius ($\sigma_r/l_0 = 1 - 0.1$) from the plane wave theory ($\sigma_r/l_0 = \infty$) reduce as τ_d decreases. See color version of this figure in the HTML.

[24] Throughout the paper, hydrometeor particles have been assumed to be stationary in air. If the particles move around, the phase coherence between the two time reversal paths in the cross term of Figure 3 will break down, resulting in decorrelation. This problem was studied by *Akkermans et al.* [1988] and *Golubentsev* [1984] using time-dependent diffusion approximations in scalar. Although consistent derivation requires a time-dependent Green function, we can roughly estimate the limit of the results in the present paper. Suppose that v is a dominant particle velocity on average. The travel time of the radar wave in the process of the second-order scattering (Figure 3c) can be written $T \approx l_0/c$ with the velocity of light c and the mean free path l_0. During time T, two scatterers move over a total distance $L \approx 2\, v\, l_0/c$. *Akkermans et al.* [1988] proved that the backscattering enhancement is observable, as long as the condition $L \ll \lambda$ is satisfied, which can be rewritten in the form of

$$l_0[m] \ll 4.5 \times 10^7 (v\,[m/sec] f\,[\mathrm{GHz}])^{-1} \qquad (34)$$

For an extremely fast wind $v \approx 100$ m/sec with $f = 95$ GHz, equation (34) gives $l_o \ll 4800$ m. This condition is generally satisfied when the multiple scattering is significant in hydrometeors.

4. Conclusions

[25] In this paper, a vector theory, including up to the second-order scattering, has been studied for continuous wave incidence as a time-independent theory. A single layer of hydrometeors has been assumed to be composed of spherical water drops of diameter D with a uniform density N_0. A Gaussian antenna pattern along with spherical wave has been introduced to take a finite footprint radius into account. For a given footprint radius and the mean free path in a random medium, the multiple-scattering reflectivity becomes smaller than the value predicted by the plane wave theory. This reduction becomes more significant as the optical thickness of hydrometeors increases, its exact value depending on the ratio of mean free path to radar footprint radius as shown in Figure 9 for the case of $D = 1$ mm. Although the dependence on the particle density N_0 does not appear explicitly in Figure 9, it is implicitly included in the mean free path l_0 as shown in Figure 8.

[26] Since the theory in this paper is derived as a time-independent theory, it can be applied only to the stationary process such as CW radars (not FM-CW radars). To apply for pulsed radars, the theory must be extended to a time-dependent theory. For a single layer of hydrometeors, an analytical solution of the time-dependent radiative transfer theory was derived for the plane wave incidence by *Ito et al.* [1995], based on generalized spherical harmonics expansions [*Oguchi*, 1980; *Ito and Oguchi*, 1987, 1989]. However their approach does not include the effects of the second-order cross term (backscattering enhancement) nor the finite beam width. A promising approach is therefore to combine the formalism of *Ito et al.* [1995] with that of the present paper. To develop this algorithm, raindrops are more tractable than ice particles. Since the shape of raindrops is close to sphere, large LDR values, such as measured in the Ka band range by *Ito et al.* [1995] and *Iguchi et al.* [1992], can be attributed to multiple-scattering effect rather than to nonspherical particle effect. This issue will be studied in the future. On the other hand, when the vertical range resolution l_{res}(= cT/2) is larger than the mean free path l_{free}, that is, $l_{res} > l_{free}$, the theory of this paper can be used to estimate the amount of second-order scattering near the top surface of hydrometeors as discussed in section A3.

[27] In addition to developing a time-dependent algorithm, it is also necessary to include effects of a generic drop size distribution (DSD), and nonspherical particles. Since the former effect breaks the high symmetrical forms of the scattering amplitude matrices in equations (16) and (17) because of the lack of symmetry for particle exchange,

a new formalism must be developed. The latter effect is also important especially for ice particles in clouds, which often are represented as needles (columns) and plates. The nonsphericity of these particles will introduce spatial anisotropy both in the scattering amplitude matrix and in the propagation Green function. Once these two effects are introduced into the formalism, the second-order scatterings for ice particles can be easily calculated, which is of main interest for W band weather radars.

Appendix A: Details of Derivation

A1. Derivation of the Second-Order Ladder Term

[28] The second-order ladder term can be derived by substituting equations (1), (7), and (15) into the diagram of Figure 2a. In the course of calculation, the center mass and relative coordinates are introduced in the same manner as the previous works [*Mandt et al.*, 1990; *Ishimaru and Tsang*, 1988; *Tsang and Kong*, 2001]:

$$\mathbf{r}_\perp = \mathbf{r_a}_\perp - \mathbf{r_b}_\perp \tag{A1}$$

$$\mathbf{r_{ce}}_\perp = (\mathbf{r_a}_\perp + \mathbf{r_b}_\perp)/\mathbf{2} \tag{A2}$$

in which $\mathbf{r_a}_\perp$ and $\mathbf{r_b}_\perp$ denote the transverse components of position vectors $\mathbf{r_a}$ and $\mathbf{r_b}$. Theses transformations lead the second-order ladder term to the form of

$$I_L^{(2)} = \pi P_t G_0^2 N_0^2 \sigma_r^2 / \left(4k^2 r_s\right) \int_{-d}^{0} dz_a \int_{-d}^{0} dz_b \cdot \exp\left[2\kappa_{iz}'' z_b + 2\kappa_{sz}'' z_a\right] J(z_a, z_b) \tag{A3}$$

In equation (A3), the function $J(z_a, z_b)$ can be represented in the following form along with the transformations of

$$x_\perp = (z_a - z_b)\ \tan\theta\ \cos\varphi \tag{A4}$$

$$y_\perp = (z_a - z_b)\ \tan\theta\ \sin\varphi \tag{A5}$$

For $z_a > z_b$

$$J(z_a, z_b) = \int_0^{\pi/2} d\theta\ \tan\theta \int_0^{2\pi} d\varphi \cdot \exp\left[-(z_a - z_b)^2 \tan^2\theta / 4\sigma_r^2\right] \cdot \exp[-\kappa_e (z_a - z_b)\sec\theta] \cdot \sum_{\hat{\alpha}} \left| \left\langle \hat{\alpha} \middle| F\left(\hat{k}_s, \hat{r}\right) F\left(\hat{r}, \hat{k}_i\right) \middle| \psi_0 \right\rangle \right|^2 \tag{A6}$$

while for $z_a < z_b$

$$J(z_a, z_b) = \int_0^{\pi/2} d\theta\ \tan\theta \int_0^{2\pi} d\varphi \cdot \exp\left[-(z_a - z_b)^2 \tan^2\theta / 4\sigma_r^2\right] \cdot \exp[\kappa_e (z_a - z_b)\sec\theta] \cdot \sum_{\hat{\alpha}} \left| \left\langle \hat{\alpha} \middle| F\left(\hat{k}_s, -\hat{r}\right) F\left(-\hat{r}, \hat{k}_i\right) \middle| \psi_0 \right\rangle \right|^2 \tag{A7}$$

Up to this point, there is no substantial difference from *Mandt et al.* [1990]. Since we cannot calculate analytically the integrals over z_a and z_b for the case of finite beam width as was done for the plane wave case, further simplification is to be introduced through the following transformations:

$$\zeta = z_a - z_b \tag{A8}$$

$$\zeta' = (z_a + z_b)/2 \tag{A9}$$

Noting the relations satisfied for a general function $g(z_a, z_b)$:

$$\begin{cases} \int_{-d}^{0} dz_a \int_{-d}^{0} dz_b g(z_a, z_b) = \int_0^d d\zeta \int_{-d+\zeta/2}^{-\zeta/2} d\zeta' g(\zeta, \zeta') & \text{for } z_a > z_b \\ \int_{-d}^{0} dz_a \int_{-d}^{0} dz_b g(z_a, z_b) = \int_0^d d\zeta \int_{-d+\zeta/2}^{-\zeta/2} d\zeta' g(-\zeta, \zeta') & \text{for } z_a < z_b \end{cases} \tag{A10}$$

we obtain the form of

$$\begin{aligned} I_L^{(2)} = {} & P_t G_0^2 \lambda^2 \theta_d^2 \left(2^7 \pi\ \ln 2\, r_s^2\right)^{-1} N_0^2 \left\{2\left(\kappa_{iz}'' + \kappa_{sz}''\right)\right\}^{-1} \\ & \cdot \int_0^{\pi/2} d\theta\ \tan\theta \int_0^{2\pi} d\varphi \int_0^d d\zeta \\ & \cdot \exp[-\kappa_e \zeta\ \sec\theta]\ \exp\left[-\zeta^2 \tan\theta / 4\sigma_r^2\right] \\ & \cdot \sum_{\hat{\alpha}} \left\{ \left| \left\langle \hat{\alpha} \middle| F\left(\hat{k}_s, \hat{r}\right) F\left(\hat{r}, \hat{k}_i\right) \middle| \psi_0 \right\rangle \right|^2 \right. \\ & \cdot \left[\exp\left\{-2\kappa_{iz}'' \zeta\right\} - \exp\left\{2\kappa_{sz}'' \zeta - 2\left(\kappa_{iz}'' + \kappa_{sz}''\right) d\right\}\right] \\ & + \left| \left\langle \hat{\alpha} \middle| F\left(\hat{k}_s, -\hat{r}\right) F\left(-\hat{r}, \hat{k}_i\right) \middle| \psi_0 \right\rangle \right|^2 \\ & \left. \cdot \left[\exp\left\{-2\kappa_{sz}'' \zeta\right\} - \exp\left\{2\kappa_{iz}'' \zeta - 2\left(\kappa_{iz}'' + \kappa_{sz}''\right) d\right\}\right] \right\} \end{aligned} \tag{A11}$$

Finally conversion of the integral variable θ to $\eta = \tan\theta$ leads to equation (16).

A2. Spatial Anisotropy of Ladder and Cross Terms

[29] Suppose that a scattering plane is parallel to the polarization $\hat{v}$. When the initial polarization ψ_0 is parallel(orthogonal) to $\hat{v}$, this condition is referred to as parallel(orthogonal) angular displacement. Difference

between the parallel and orthogonal angular displacements appear only through the terms $\langle\hat{\alpha}|F(\hat{k}_s, \pm\hat{r})\ F(\pm\hat{r}, \hat{k}_i)|\psi_0\rangle$ in equations (16) and (17). Throughout this section, it is noted that equation (28) is approximately satisfied with high accuracy for $|\theta_s| \lessapprox 0.1°$.

A2.1. Proof of $L_2^{co}(\hat{v}\hat{v}) = L_2^{co}(\hat{h}\hat{h})$

[30] Since equation (28) is well satisfied for $|\theta_s| \lessapprox 0.1°$,

$$\left|\left\langle\hat{v}\middle|F\left(\hat{k}_s, \hat{r}\right)\ F\left(\hat{r}, \hat{k}_i\right)\middle|\hat{v}\right\rangle\right|^2 = 2^{-1}|a|^2 + |b|^2 + 2^{-1}|a|^2\cos 4\varphi + (ab^* + ba^*)\cos 2\varphi \tag{A12}$$

$$\left|\left\langle\hat{h}\middle|F\left(\hat{k}_s, \hat{r}\right)\ F\left(\hat{r}, \hat{k}_i\right)\middle|\hat{h}\right\rangle\right|^2 = 2^{-1}|a|^2 + |b|^2 + 2^{-1}|a|^2\cos 4\varphi - (ab^* + ba^*)\cos 2\varphi \tag{A13}$$

Using equations (A12) and (A13), we can show

$$\int d\varphi\left|\left\langle\hat{v}\middle|F\left(\hat{k}_s, \hat{r}\right)\ F\left(\hat{r}, \hat{k}_i\right)\middle|\hat{v}\right\rangle\right|^2 = \int d\varphi\left|\left\langle\hat{h}\middle|F\left(\hat{k}_s, \hat{r}\right)\ F\left(\hat{r}, \hat{k}_i\right)\middle|\hat{h}\right\rangle\right|^2 \tag{A14}$$

which is also satisfied for $-\hat{r}$. Noting that the integral over φ in equation (16) concerns only to the terms $\langle\hat{\alpha}|F(\hat{k}_s, \pm\hat{r})\ F(\pm\hat{r}, \hat{k}_i)|\psi_0\rangle$, the substitution of equation (A14) and its counterpart for $-\hat{r}$ into equation (16) yields

$$I_L^{(2)}(\hat{v}\hat{v}) = I_L^{(2)}\left(\hat{h}\hat{h}\right) \tag{A15}$$

For the nearly backscattering $|\theta_s| \lessapprox 0.1°$, the following relation is approximately satisfied for the spherical particle with high accuracy:

$$I_L^{(1)} \equiv I_L^{(1)}(\hat{v}\hat{v}) \approx I_L^{(1)}\left(\hat{h}\hat{h}\right) \tag{A16}$$

We divide equation (A15) by equation (A16) to obtain

$$L_2^{co}(\hat{v}\hat{v}) = L_2^{co}\left(\hat{h}\hat{h}\right) \tag{A17}$$

Equation (A17) means that the reflectivity of the second-order ladder term in copolarization from $\hat{v}$ to $\hat{v}$ is equal to that from $\hat{h}$ to $\hat{h}$ as shown by the dash-dotted line in Figure 5a.

A2.2. Spatial Anisotropy of the Cross Term in Copolarized Return

[31] Since equation (28) is well satisfied for $|\theta_s| \lessapprox 0.1°$, we derive

$$\left\langle\hat{v}\middle|F\left(\hat{k}_s, \hat{r}\right)\ F\left(\hat{r}, \hat{k}_i\right)\middle|\hat{v}\right\rangle^*\left\langle\hat{v}\middle|F\left(\hat{k}_s, -\hat{r}\right)\ F\left(-\hat{r}, \hat{k}_i\right)\middle|\hat{v}\right\rangle = 2^{-1}a^*a' + b^*b' + 2^{-1}a^*a'\cos 4\varphi + (a^*b' + b^*a')\cos 2\varphi \tag{A18}$$

in which a' and b' correspond to the values a and b in equations (29) and (30) by replacing θ with $\pi - \theta$. In the same manner,

$$\left\langle\hat{h}\middle|F\left(\hat{k}_s, \hat{r}\right)\ F\left(\hat{r}, \hat{k}_i\right)\middle|\hat{h}\right\rangle^*\left\langle\hat{h}\middle|F\left(\hat{k}_s, -\hat{r}\right)\ F\left(-\hat{r}, \hat{k}_i\right)\middle|\hat{h}\right\rangle = 2^{-1}a^*a' + b^*b' + 2^{-1}a^*a'\cos 4\varphi - (a^*b' + b^*a')\cos 2\varphi \tag{A19}$$

Substituting equation (A18) and (A19) along with equation (22) into the integral over φ in equation (17), we obtain for the $\theta_s = 0$:

$$\begin{aligned}&\int d\varphi Re\left\{\left\langle\hat{v}\middle|F\left(\hat{k}_s, \hat{r}\right)\ F\left(\hat{r}, \hat{k}_i\right)\middle|\hat{v}\right\rangle^* \cdot\left\langle\hat{v}\middle|F\left(\hat{k}_s, -\hat{r}\right)\ F\left(-\hat{r}, \hat{k}_i\right)\middle|\hat{v}\right\rangle\exp[i(k_{dz} + t)\zeta]\right\}\\ &= \int d\varphi Re\left\{\left\langle\hat{h}\middle|F\left(\hat{k}_s, \hat{r}\right)\ F\left(\hat{r}, \hat{k}_i\right)\middle|\hat{h}\right\rangle^* \cdot\left\langle\hat{h}\middle|F\left(\hat{k}_s, -\hat{r}\right)\ F\left(-\hat{r}, \hat{k}_i\right)\middle|\hat{h}\right\rangle\exp[i(k_{dz} + t)\zeta]\right\}\end{aligned} \tag{A20}$$

which leads to

$$I_C^{(2)}(\hat{v}\hat{v}) = I_C^{(2)}\left(\hat{h}\hat{h}\right) \tag{A21}$$

Dividing both sides by equation (A16), we obtain

$$C_2^{co}(\hat{v}\hat{v}) = C_2^{co}\left(\hat{h}\hat{h}\right) \tag{A22}$$

Equation (A22) is satisfied only for the backscattering direction $\theta_s = 0$ because of the lack of the oscillation term $\exp[i(k_{dz} + t)\zeta]$. For $\theta_s \neq 0$, the term $\exp[i(k_{dz} + t)\zeta]$ gives another dependence on the integral variable φ, and equation (A22) is no longer satisfied. This is the origin of the spatial anisotropy of the backscattering enhancement in copolarization as shown by the two solid lines in Figure 5a.

A2.3. Proof of $L_2^{cx}(\hat{v}\hat{h}) = L_2^{cx}(\hat{h}\hat{v})$ and $C_2^{cx}(\hat{v}\hat{h}) = C_2^{cx}(\hat{h}\hat{v})$

[32] These properties can be easily derived for the nearly backscattering $|\theta_s| \lessapprox 0.1°$ by substituting equation (31) and its counterpart for $-\hat{r}$ into equation (17), followed by dividing by equation (A16). The equalities/isotropies $L_2^{cx}(\hat{v}\hat{h}) = L_2^{cx}(\hat{h}\hat{v})$, and $C_2^{cx}(\hat{v}\hat{h}) = C_2^{cx}(\hat{h}\hat{v})$ are represented in Figure 5b.

A3. Special Condition to Apply the Time-Independent Theory to Pulsed Radars

[33] Although the returned signals due to the second-order scattering represented by equations (16) and (17) have been derived as time independent process such as CW radars (not FM-CW radars), it is worth comparing the scheme represented by these equations with that of pulsed radars. Figure A1 is a bounce diagram [*Bringi*

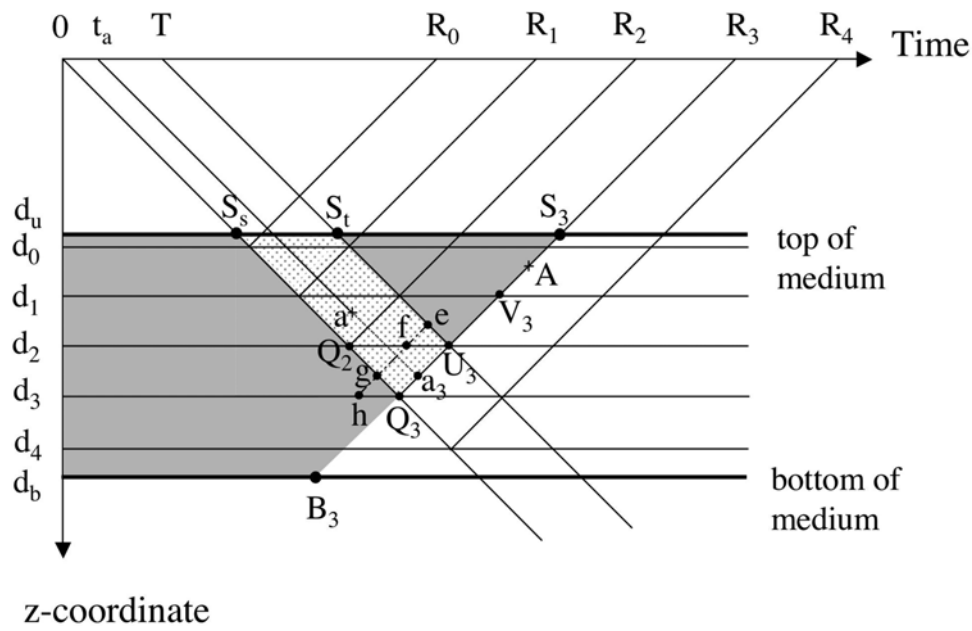

Figure A1. Bounce diagram. The speed of light c is set at unity. A uniform random medium exists from the range d_u to d_b. The leading and trailing edges of pulses are transmitted at times 0 and T, respectively.

and Chandrasekar, 2001; *Freeman*, 1996]. Since this diagram is a projection of four dimensional spaces into two dimensional spaces of z coordinate (range) and time, we cannot fully represent information on multiple scattering, but it is still useful. In the diagram, the speed of light is set at unity, so that the time and z coordinate are plotted in the same scale. Suppose that a uniform random medium exists between the ranges d_u and d_b, and that the leading and trailing edges of a pulse are transmitted at time 0 and T respectively. Then the signal representing the range d_3 is received at time R_3, including the first-order scattering contribution from the line Q_3U_3. When considering the second-order scattering process, a ray scattered first at any point in the dotted region has possibility to be secondly scattered at a certain point on the line Q_3S_3, eventually being received at time R_3. For instance, if an incident ray transmitted at time t_a is scattered at point "a," a second-time scattering can occur at a certain point "A" on the line a_3S_3, as long as the three dimensional distance between points "a" and "A" is properly chosen. It is therefore seen that even for pulsed radars, multiple-scattering effect contaminates into the signal of a given range. However, the contribution of second-order scattering comes only from the dotted region. On the other hand, the time-independent theory, referred to as CW radars, includes the contribution of the second-order scattering from both the solid gray and dotted regions, and at the same time, the first-order scattering comes from all the points on the line B_3S_3. Hence it is challenging to generalize the comparison of the effects of second order scattering between these two schemes. However in the case of $l_{res} > l_{free}$, where l_{res} and l_{free} are the range resolution (cT/2) and the mean free path of medium respectively, the amounts of second order scattering in both the pulsed and CW radars can be considered roughly equal near the top surface of hydrometeors. This will be explained by using the bounce diagram, in which the dash-dotted line "eh" is drawn with $U_3f = Q_3h = l_{free}$. Then the contribution of the second-order scattering for pulsed radars can be considered to come roughly from the region "U_3egQ_3," while for CW radars applied only between d_2 and d_3 (i.e., the integral limit "d" in equations (16) and (17) is replaced with $l_{res} = d_3 - d_2$), the contribution comes from the region "U_3fhQ_3." Among these regions, the triangle "efU_3" for pulsed radars contributes to more amount of second-order scattering onto the line "Q_3V_3" than the triangle "ghQ_3" for CW radars does, because the larger range suffers more absorption. A small portion of the shared region "U_3fgQ_3" may also give slight contribution of second-order scattering to the line "U_3V_3" for pulsed radars. Furthermore as the range increases, the second-order contributions from regions other than "U_3egQ_3" for pulsed radars will be no longer negligible. As seen from the bounce diagram, these difference-causing effects will be reduced near the top surface. It is thus seen that the second-order scattering

calculated from the time-independent theory, applied to the ranges d_2 and d_3, is a good estimation for pulsed radars under the condition of $l_{res} > l_{free}$, only if the range $d_2 - d_3$ is located near the top surface, that is, for the range $d_0 - d_1$.

[34] On the contrary, for $l_{res} < l_{free}$, especially for $2l_{res} < l_{free}$, more contribution of the second-order scattering comes from the dotted region "$U_3Q_2S_sS_t$" for pulsed radars, while for CW radars, from the solid gray region "$Q_2d_2d_3Q_3$." In addition, for pulsed radars, the contribution from the region "$U_3Q_2Q_3$" to the line U_3S_3 will increase. It is again difficult to evaluate the amounts of these second-order scattering for pulsed radars through the formalism of this paper, and the time-dependent algorithm is needed.

[35] Summarizing the case of $l_{res} > l_{free}$, the formalism of this paper can roughly estimate the amount of second-order scattering of pulsed radars in ranges near the top surface. Our preliminary calculation showed that the mean free path l_{free} is between 300 and 500 meter for rains of 10 mm/hr, depending on drop size distributions. Since the range resolution of the CloudSat and EarthCare missions is 500 meter, the above condition is weakly satisfied.

[36] **Acknowledgments.** The research described in this paper was carried out at the Jet Propulsion Laboratory, California Institute of Technology, under a contract with the National Aeronautics and Space Administration. The authors thank Tomohiro Oguchi at Kanto Gakuin University, Shigeo Ito at Toyo University, Toshio Iguchi at National Institute of Information and Communications Technology, and Hajime Okamoto at Tohoku University for elaborate advice and suggestions.

References

Akkermans, E., P. E. Wolf, and R. Maynard (1986), Coherent backscattering of light by disordered media: Analysis of the peak line shape, *Phys. Rev. Lett.*, *56*, 1471–1474.

Akkermans, E., P. E. Wolf, R. Maynard, and G. Maret (1988), Theoretical study of the coherent backscattering of light by disordered media, *J. Phys.*, *49*, 77–98.

Barbanenkov, Y. N., and V. D. Ozrin (1988), Coherent enhancement of back-scattered radiation in a randomly inhomogeneous medium: The diffusion approximation, *Soviet Phys. JETP*, Engl. Transl., *67*, 1117–1121.

Barbanenkov, Y. N., Y. A. Kravtsov, V. D. Ozrin, and A. I. Saichev (1991), Enhanced backscattering: The universal wave phenomenon, *Proc. IEEE*, *79*, 1367–1370.

Bringi, V. N., and V. Chandrasekar (2001), *Polarimetric Doppler Weather Radar*, chap. 5, pp. 211–293, Cambridge Univ. Press, New York.

de Wolf, D. A. (1971), Electromagnetic reflection from an extended turbulent medium: Cumulative forward scatter single-backscatter approximation, *IEEE Trans. Antennas Propag.*, *19*, 254–262.

de Wolf, D. A., W. J. Russchenberg, and L. P. Ligthart (2000), Radar reflection from clouds: Gigahertz backscatter cross sections and Doppler spectra, *IEEE Trans. Antennas Propag.*, *48*, 254–259.

Freeman, J. C. (1996), *Fundamentals of Microwave Transmission Lines*, chap. 2, pp. 52–131, Wiley-Interscience, Hoboken, N. J.

Golubentsev, A. A. (1984), Suppression of interference effects in multiple scattering of light, *Soviet Phys. JETP*, Engl. Transl., *59*, 26–32.

Iguchi, T., R. Meneghini, and H. Kumagai (1992), Radar depolarization signatures of rains in cumulus clouds measured with dual-frequency air-borne radar, paper presented at 1992 International Geoscience and Remote Sensing Symposium, IEEE Geosci. and Remote Sens. Soc., Houston, Tex.

Ishimaru, A. (1991), Backscattering enhancement: From radar cross sections to electron and light localizations to rough surface scattering, *IEEE Antennas Propag. Mag.*, *33*, 7–11.

Ishimaru, A., and L. Tsang (1988), Backscattering enhancement of random discrete scatterers of moderate sizes, *J. Opt. Soc. Am. A Opt. Image Sci.*, *5*, 228–236.

Ito, S., and T. Oguchi (1987), An approximate method for solving radiative transfer equation in discrete random media, *Radio Sci.*, *22*, 873–879.

Ito, S., and T. Oguchi (1989), Approximate solutions of the vector radiative transfer equation for linearly polarized light in discrete random media, *J. Opt. Soc. Am. A Opt. Image Sci.*, *6*, 1852–1858.

Ito, S., T. Oguchi, T. Iguchi, H. Kumagai, and R. Meneghini (1995), Depolarization of radar signals due to multiple scattering in rain, *IEEE Trans. Geosci. Remote Sens.*, *33*, 1057–1062.

Kobayashi, S. (2002), A unified formalism of incoherent, quasi-coherent and coherent correlation signals on pulse-pair Doppler operation: Aiming for cloud-profiling radar for a space mission, *J. Atmos. Oceanic Technol.*, *19*, 443–456.

Kravtsov, Y., and A. I. Saichev (1982), Effects of double passage of waves in randomly inhomogeneous media, *Sov. Phys. Usp.*, *25*, 494–508, Engl. Transl.

Kuga, Y., and A. Ishimaru (1984), Retroreflectance from a dense distribution of spherical particles, *J. Opt. Soc. Am. A Opt. Image Sci.*, *1*, 831–835.

Kuzmin, V. L., V. P. Romanov, and V. L. Kuzmin (1992), Depolarization of coherent backscattering, *Opt. Spectrosc.*, *72*, 125–130.

Lure, Y. M., C. C. Yang, and K. C. Yeh (1989), Enhanced backscattering phenomenon in a random continuum, *Radio Sci.*, *24*, 147–159.

Mandt, C. E., and L. Tsang (1992), Backscattering enhancement from a random distribution of large discrete spherical scatterers with a size distribution, *J. Opt. Soc. Am. A Opt. Image Sci.*, *9*, 2246–2251.

Mandt, C. E., L. Tsang, and A. Ishimaru (1990), Copolarized and depolarized backscattering enhancement of random discrete scatterers of large size based on second-order ladder

and cyclical theory, *J. Opt. Soc. Am. A Opt. Image Sci.*, *7*, 585–592.

Mishchenko, M. I. (1991), Polarization effects in weak localization of light: Calculation of the copolarized and depolarized backscattering enhancement factors, *Phys. Rev. B*, *44*, 12,597–12,600.

Mishchenko, M. I. (1992), Enhanced backscattering of polarized light from discrete random media: Calculations in exactly the backscattering direction, *J. Opt. Soc. Am. A Opt. Image Sci.*, *9*, 978–982.

Oguchi, T. (1973), Attenuation and phase rotation of radio waves due to rain: Calculations at 19.3 and 34.8 GHz, *Radio Sci.*, *8*, 31–38.

Oguchi, T. (1980), Effect of incoherent scattering on attenuation and cross polarization of millimeter wave due to rain: Preliminary calculations at 34.8 GHz and 82 GHz for spherical raindrops, *J. Radio Res. Lab.*, *27*, 1–51.

Oguchi, T., and T. Ihara (2005), Enhanced backscattering from randomly distributed spherical scatterers at 30 GHz: Computer simulation and comparison with measurement, paper presented at 2005 International Symposium on Antennas and Propagation, Korea Electromagn. Eng. Soc., Seoul, Korea.

Saxon, D. S. (1955), Tensor scattering matrix for the electromagnetic field, *Phys. Rev.*, *100*, 1771–1775.

Stephen, M. J., and G. Cwilich (1986), Rayleigh scattering and weak localization: Effect of polarization, *Phys. Rev. B.*, *34*, 7564–7572.

Tazaki, T., H. Tabuchi, K. Ikeda, T. Oguchi, and S. Ito (2000), Laboratory measurements of polarimetric radar signatures of randomly distributed spherical and spheroidal scatterers at 30 GHz, *IEE Proc. Microwave Antennas Propag.*, *147*, 8–12.

Tsang, L., and A. Ishimaru (1984), Backscattering enhancement of random discrete scatterers, *J. Opt. Soc. Am. A Opt. Image Sci.*, *1*, 836–839.

Tsang, L., and A. Ishimaru (1985), Theory of backscattering enhancement of random discrete isotropic scatterers based on the summation of all ladder and cyclical terms, *J. Opt. Soc. Am. A Opt. Image Sci.*, *2*, 1331–1338.

Tsang, L., and J. A. Kong (2001), *Scattering of Electromagnetic Waves: Advanced Topics*, chap. 8, pp. 359–405, John Wiley, Hoboken, New York.

van Albada, M. P., and A. Lagendijk (1987), Vector character of light in weak localization: Spatial anisotropy in coherent backscattering from a random medium, *Phys. Rev. B.*, *36*, 2353–2356.

van Albada, M. P., M. B. van der Mark, and A. Lagendijk (1987), Observation of weak localization of light in a finite slab: Anisotropy effects and light-path classification, *Phys. Rev. Lett.*, *58*, 361–364.

van Bladel, J. (1961), Some remarks on Green's dyadic for infinite space, *IRE Trans. Antennas Propag.*, *9*, 563–566.

Wolf, P. E., and G. Maret (1985), Weak localization and coherent backscattering of photons in disordered media, *Phys. Rev. Lett.*, *55*, 2696–2699.

E. Im, S. Kobayashi, and S. Tanelli, Jet Propulsion Laboratory, California Institute of Technology, 4800 Oak Grove Dr., MS 300-243, Pasadena, CA 91109, USA. (satoru@radar-sci.jpl.nasa.gov)